JACS
JOURNAL OF THE AMERICAN CHEMICAL SOCIETY

Perspective

pubs.acs.org/JACS

# Epitaxial Growth of Hetero-Nanostructures Based on Ultrathin Two-Dimensional Nanosheets

Chaoliang Tan and Hua Zhang*

School of Materials Science and Engineering, Nanyang Technological University, 50 Nanyang Avenue, Singapore 639798, Singapore

**ABSTRACT:** Ultrathin two-dimensional (2D) nanosheets, such as graphene and $MoS_2$, which are demonstrated to be fundamentally and technologically important in many applications, have emerged as a unique family of nanomaterials in chemistry and material science over the past decade. The single-crystalline nature and ultrathin thickness of these 2D nanosheets make them ideal templates for the epitaxial deposition of nanostructures, which offer many possibilities to engineer microsized 2D p−n hetero-junctions at atomic/nanometer scale. This Perspective aims to provide information on the epitaxial growth of hetero-nanostructures based on ultrathin 2D nanosheets. Various methods for the epitaxial growth of nanostructures based on ultrathin 2D nanosheets or in situ growth of lateral or vertical epitaxial 2D semiconductor hetero-nanostructures are introduced. The advantages of these 2D epitaxial hetero-nanostructures for some applications, such as electronics, optoelectronics, and electrocatalysis, are also presented. On the basis of the current status of 2D epitaxial hetero-nanostructures, the future prospects of this promising area are discussed.

## INTRODUCTION

Epitaxial growth is the deposition of one kind of crystals on the crystal face of another crystalline substrate, in which the deposited crystal has the same structural orientation with the crystalline substrate.[1] Generally, substrates used for epitaxial growth are highly crystalline bulk substrates with a single exposed facet, such as graphite, mica, Si(111), and Au(111).[1−5] Epitaxially grown thin films and nanostructures have shown superior performance in a wide range of applications, including plasmonics, electronics, optoelectronics, and catalysis, owning to their well-defined structure/interface or selectively exposed facets.[1−5] Benefiting from the advantages of nanomaterials, engineering epitaxial hetero-nanostructures is believed to enable them with some interesting optical, chemical, and electronic properties and functions due to the epitaxial growth nature.[6] Currently, the construction of epitaxial hetero-nanostructures is normally based on the formation of epitaxial core−shell nanoparticles (NPs)/nanowires or epitaxial deposition of NPs on another sort of nanocrystals (e.g., nanowires, nanorods, and nanocubes).[7−15] As a class of newly emerging nanomaterials, ultrathin two-dimensional (2D) nanosheets, in particular graphene and layered transition metal dichalcogenides (TMDs), have attracted considerable attention in recent years and shown promising potential in various applications, such as electronics/optoelectronics, catalysis, energy storage and conversion, sensing, and biomedicine.[16−27] Moreover, engineering functional hybrid nanostructures based on ultrathin 2D nanosheets has been demonstrated to be a fascinating strategy to modulate the chemical and electronic properties of 2D nanosheets.[28−30] These ultrathin 2D nanosheets, despite being atomically thin, still keep the single-crystalline feature, making them ideal templates for epitaxial deposition of nanostructures. Of particular interest is that the solution-processability of some ultrathin 2D nanosheets allows for the epitaxial growth of hetero-nanostructures in the liquid phase in high yield and on a large scale. The ultrathin feature and large lateral size also offer opportunities to engineer microsized 2D p−n hetero-junctions at atomic/nanometer scale.

In this Perspective, we will focus on the discussion of the recent progress on epitaxial growth of hetero-nanostructures based on ultrathin 2D nanosheets. The epitaxial growth of other nanostructures, such as topological insulators and $MoS_2$, on graphene will first be introduced. Then, how to achieve the epitaxial growth of lateral and vertical hetero-junctions of TMD monolayers will be demonstrated. Moreover, we will describe the recent achievements in liquid-phase epitaxial growth of nanostructures on ultrathin 2D semiconductor nanosheets as well as the preparation of epitaxial core−shell noble metal nanosheets. After that, we will highlight the advantages of these resultant epitaxially grown hetero-nanostructures for a number of applications, such as electronics, optoelectronics, and electrocatalysis. Finally, on the basis of conclusions on the current research achievement, the challenges and our personal perspective of the future research directions in this research area will be laid out, aiming to inspire more exciting studies in the near future.

## EPITAXIAL GROWTH OF 2D NANOSTRUCTURES ON GRAPHENE SHEETS

Graphene, the most studied ultrathin 2D nanosheet over the past decade, is an atomically thin carbon monolayer consisting of $sp^2$ carbon atoms compacted into a 2D honeycomb lattice.[31] Graphite is one of the most widely used substrates for epitaxial growth of other materials, such as organic crystals, noble metals, and semiconductors.[1,2] Since graphene is the basic building block of graphite, we can predict that graphene, especially the pristine and chemical vapor deposition (CVD)-grown one, could also be a promising template for epitaxial growth of other nanomaterials due to its similar crystalline and surface feature with graphite.

To date, several kinds of nanostructures, such as topological insulator nanoplates (e.g., $Bi_2Se_3$ and $In_2Se_3$), $MoS_2$, $WSe_2$, and hexagonal boron nitride (h-BN) nanosheets, have been

**Received:** April 7, 2015
**Published:** September 15, 2015




DOI: 10.1021/jacs.5b03590
J. Am. Chem. Soc. 2015, 137, 12162−12174

**Table 1. Summary of the Epitaxial Hetero-Nanostructures Based on Ultrathin 2D Nanosheets**

| 2D epitaxial hetero-structure | synthesis method | type of epitaxial hetero-structure | application | ref |
|---|---|---|---|---|
| $Bi_2Se_3$–graphene | vapor-phase deposition | $Bi_2Se_3$ nanosheets grown on few-layer graphene | – | 32 |
| $In_2Se_3$–graphene | van der Waals epitaxy | $In_2Se_3$ patterns with different shapes grown on graphene | photodetectors | 33 |
| $MoS_2$–graphene | CVD | $MoS_2$ nanosheets grown on graphene | – | 34 |
| $MoS_2$–graphene, $WSe_2$–graphene, h-BN–graphene | CVD | $MoS_2$, $WSe_2$, and h-BN nanosheets grown graphene | photodetectors | 35 |
| $WSe_2$-graphene | CVD and MOCVD | triangular $WSe_2$ nanosheets grown graphene | – | 36 |
| $MoS_2$–$MoSe_2$, $WS_2$–$WSe_2$ | CVD | lateral hetero-structures | CMOS inverters | 51 |
| $MoSe_2$–$WSe_2$ | CVD | lateral hetero-structures | – | 52 |
| $WS_2$–$MoS_2$ | CVD | lateral and vertical hetero-structures | photodiodes and FETs | 53 |
| $MoS_2$–$WS_2$ | CVD | lateral and vertical hetero-structures | – | 54 |
| $MoS_2$–$WS_2$ | CVD | vertical hetero-structures | – | 55 |
| $MoS_2$–$WS_2$, $MoSe_2$–$WSe_2$ | ambient-pressure CVD | lateral hetero-structures | – | 56 |
| $WSe_2$–$MoSe_2$ | two-step CVD | vertical hetero-structures | – | 57 |
| $WSe_2$–$MoS_2$ | two-step CVD | lateral hetero-structures | photodiodes | 58 |
| $MoSe_2$–$MoS_2$ | CVD, electron beam lithography, and pulsed laser vaporization | patterned arrays of lateral hetero-structures | – | 59 |
| Pt–$MoS_2$, Pd–$MoS_2$, Ag–$MoS_2$ | wet-chemical synthesis | Pt and Pd NPs and Au triangular nanoplates grown on single-layer $MoS_2$ nanosheets | electrocatalytic HER | 60 |
| PbS–$MoS_2$, PbS–$WS_2$ | liquid exfoliation and hot injection method | PbS NPs grown on few-layer $MoS_2$ or $WS_2$ nanosheets | photodetectors | 62 |
| CuS–$TiS_2$, ZnS-$TiS_2$, $Ni_3S_2$–$TiS_2$ | modified electrochemical Li-intercalation and exfoliation | CuS, ZnS, or $Ni_3S_2$ nanoplates grown on $TiS_2$ nanosheets | Li ion batteries | 63 |
| Au–Ag | wet-chemical synthesis | Ag-coated Au core–shell hetero-structures | – | 68 |
| Au–Pt, Au–Pd | wet-chemical synthesis | Pt- or Pd-coated Au core–shell hetero-structures | – | 69 |

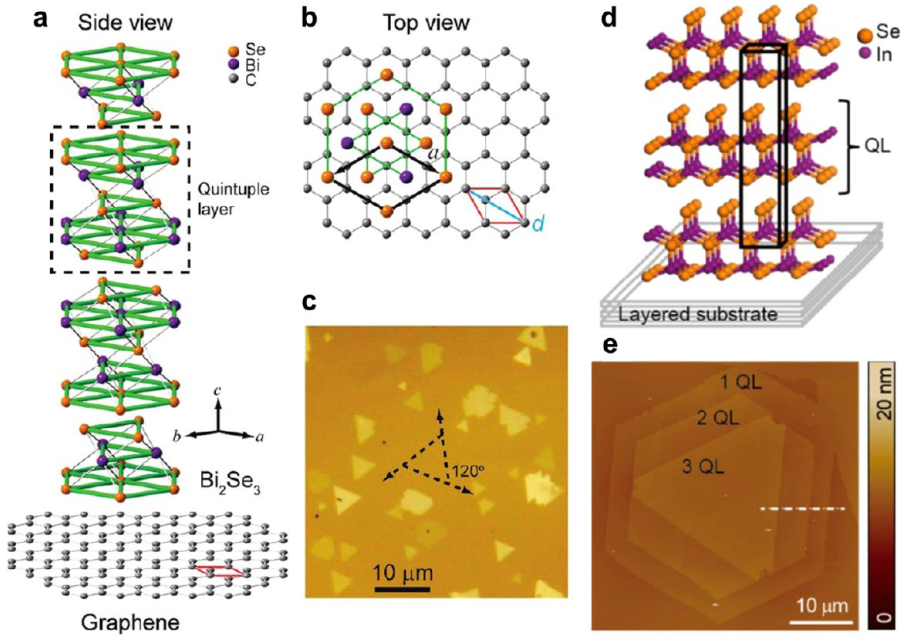


**Figure 1.** (a,b) Schematic illustration of the epitaxial growth of $Bi_2Se_3$ on graphene. (c) A typical optical image of $Bi_2Se_3$ nanoplates epitaxially grown on a multilayer graphene substrate. Reproduced with permission from ref 32. Copyright 2010, American Chemical Society. (d) Schematic illustration of $In_2Se_3$ flakes grown on a layered substrate. (e) AFM image of a terraced $In_2Se_3$ flake with thicknesses of 1–3 QLs. Reproduced with permission from ref 33. Copyright 2013, American Chemical Society.

epitaxially deposited on graphene sheets (Table 1).[32−36] Generally, the graphene used for the aforementioned epitaxial growth is mechanically exfoliated or CVD-grown, because the chemically converted graphene, such as graphene oxide (GO) and reduced graphene oxide (rGO), is unsuitable for the epitaxial growth of other nanomaterials (e.g., noble metals and semiconductors) due to its discontinuous lattice structure induced by the oxygen-containing groups on its surface.[37] As a typical example, Liu and co-workers demonstrated the epitaxial growth of $Bi_2Se_3$ nanoplates, a kind of topological insulator, on pristine few-layer graphene sheets using a simple vapor-phase deposition method (Figure 1a,b).[32] The size of grown $Bi_2Se_3$


DOI: 10.1021/jacs.5b03590
J. Am. Chem. Soc. 2015, 137, 12162−12174

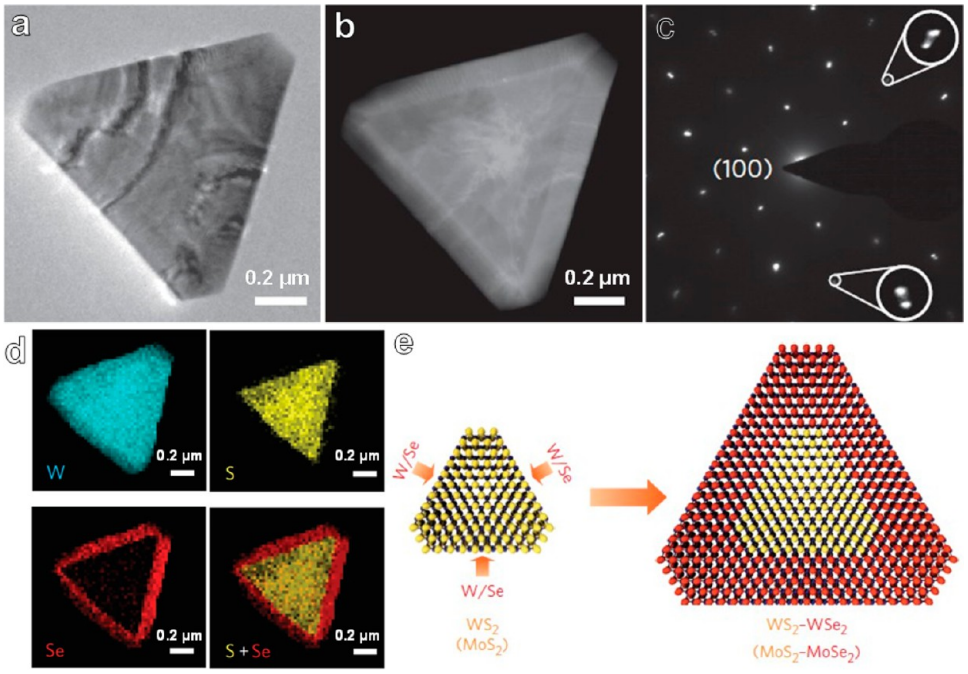


**Figure 2.** (a) TEM image of a $WSe_2$−$WS_2$ lateral hetero-nanostructure. (b) High-angle annular dark-field (HAADF) TEM image of the hetero-nanostructure. (c) SAED pattern taken across the hetero-nanostructure interface. (d) EDS elemental mapping images of $WSe_2$−$WS_2$ hetero-nanostructures. (e) Schematic illustration of lateral epitaxial growth of $WSe_2$−$WS_2$ and $MoSe_2$−$MoS_2$ hetero-nanostructures. Reproduced with permission from ref 51. Copyright 2014, Nature Publishing Group.

nanoplates is about several micrometers (Figure 1c), and the thickness can be tuned from 1 quintuple-layer (QL) to 10 QLs by varying the experimental conditions. Similarly, the same group also reported the epitaxial growth of another type of topological insulator flakers, i.e., $In_2Se_3$, with size in micrometers and atomic thickness on graphene template by the van der Waals epitaxy (Figure 1d,e).[33] The thickness, orientation, nucleation site, and crystal phase of $In_2Se_3$ flakes could be well controlled by tuning the growth condition.

Besides topological insulators, the epitaxial growth of $MoS_2$, $WSe_2$, and h-BN nanosheets on graphene has also been achieved.[34−36] For example, Kong and co-workers reported the epitaxial growth of $MoS_2$ nanosheets on CVD-grown graphene on Cu foil.[34] Briefly, the precursor for growth of $MoS_2$, i.e., $(NH_4)_2MoS_4$, in *N*,*N*-dimethylformamide was first transported onto graphene surface by a carrier gas at room temperature. Then, a relatively high temperature annealing (400 °C) was used to decompose the precursor to form $MoS_2$ sheets. The epitaxially grown $MoS_2$ sheets with a hexagonal shape on graphene own size from several hundred nanometers to several micrometers and thickness of 2−5 nm. It was found that the crystal quality of graphene is essential for the realization of epitaxial growth. In another example, Robinson and co-workers achieved the epitaxial growth of $MoS_2$, $WSe_2$, and h-BN nanosheets on CVD-grown graphene by gas-phase deposition method.[35] The used graphene is epitaxially grown on 6H-SiC substrate, making it a perfect template for epitaxy due to the lack of dangling bonds and its ability to remain intact under high stress. Note that all the aforementioned graphene-based 2D epitaxial hetero-structures are grown on rigid substrates. Very recently, Alem and co-workers reported the preparation of freestanding $WSe_2$−graphene hetero-structure by epitaxial growth of triangular monolayer $WSe_2$ with lateral size of 100−400 nm on CVD-grown graphene via the metal−organic chemical vapor deposition (MOCVD).[36]

## EPITAXIAL GROWTH OF LATERAL AND VERTICAL 2D TMD HETERO-JUNCTIONS

Besides graphene, single- and few-layer nanosheets of layered TMDs have also attracted a great deal of interest in recent years due to their 2D morphology features but different electronic properties with graphene.[17,18] In contrast to the zero band gap graphene, some of TMD monolayers (e.g., $MoS_2$, $WS_2$, $MoSe_2$, and $WSe_2$) are direct band semiconductors, holding promise for fabrication of electronic devices. For example, TMD monolayers or multilayers have shown potential as active materials for integration of transistors, phototransistors, nanogenerators, and electrical gas sensors.[38−41] It has been demonstrated that engineering van der Waals (VdW) hetero-nanostructures by simply stacking of two different kinds of ultrathin 2D nanosheets together in the vertical or lateral directions is an effective strategy to tune the electronic properties of ultrathin 2D nanosheets and thus to fully explore their potential applications in high-performance electronics and optoelectronics.[42−47] Therefore, some unusual optical and electronic properties as well as new phenomena were observed on these artificially stacked hetero-structures.[42−47] However, a transfer process is always necessary for fabrication of such kind of hetero-structures, which could introduce some polymer contaminations during the transfer process. In addition, it is also difficult to control the stacking area and orientation of the two nanosheets, making it difficult to precisely control the optical and electronic properties of the hetero-nanostructures. In contrast, the epitaxial growth of TMD monolayers to create well-defined vertical or lateral hetero-nanostructures could be an ideal approach to address the aforementioned disadvantages involved in these VdW hetero-nanostructures, allowing for precise modulation of the chemical composition and electronic properties. For realization of epitaxial growth, the lattice mismatch between the two crystals is a key factor, where lower


DOI: 10.1021/jacs.5b03590
J. Am. Chem. Soc. 2015, 137, 12162−12174

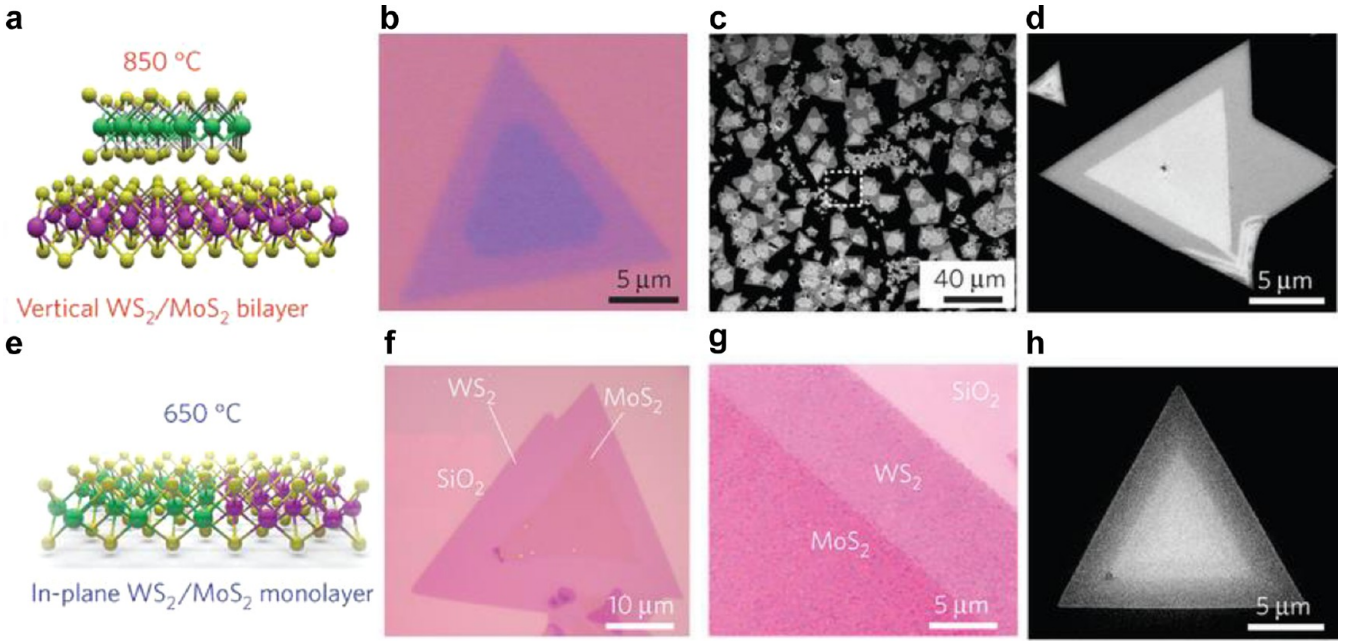


**Figure 3.** (a) Schematic illustration, (b) optical, and (c,d) SEM images of the vertical epitaxial $WS_2$−$MoS_2$ hetero-nanostructures. (e) Schematic illustration, (f,g) optical, and (h) SEM images of the lateral epitaxial $WS_2$−$MoS_2$ hetero-nanostructures. Reproduced with permission from ref 53. Copyright 2014, Nature Publishing Group.

lattice mismatch is better for epitaxial growth. Fortunately, the lattice mismatch between some TMD materials is low, which is favorable for their epitaxial growth. For example, the lattice mismatch between $MoS_2$ and $MoSe_2$ or $WS_2$ and $WSe_2$ is ∼4%.

Generally, TMD monolayers or multilayers can be grown on a silicon oxide substrate by the CVD techniques.[48,49] In principle, the preparation of lateral epitaxial hetero-nanostructure could be achieved by the successive growth of another TMD material at the edge of an existing TMD monolayer.[50] The key challenge lies in that the edge of original TMD monolayer is easily passivated after exposure to ambient conditions.[50] In this case, another TMD material tends to grow solely rather than continuously grow based on the existing TMD monolayer. Therefore, keeping a fresh, unpassivated edge is essential to achieve the successive epitaxial growth of lateral hetero-nanostructures.[50] Bearing this in mind, several kinds of gas-phase deposition methods have been developed for preparation of lateral and vertical epitaxial hetero-nanostructures consisting of two different kinds of TMD monolayers (Table 1).[51−59] As a typical example, Duan and co-workers reported the epitaxial growth of lateral hetero-nanostructures of $WSe_2$−$WS_2$ and $MoSe_2$−$MoS_2$ by the CVD method (Figure 2), in which in situ switching of the vapor-phase reactants can ensure the nonexposure of active edges to ambient conditions.[51] The as-prepared microsized hetero-nanostructures can be easily identified by optical microscopy, Raman spectroscopy, and photoluminescence mapping, transmission electron microscopy (TEM), and energy-dispersive X-ray spectroscopy (EDS) elemental mapping. For example, the TEM and EDS elemental mapping results clearly indicated the formation of $WSe_2$−$WS_2$ lateral epitaxial hetero-nanostructure (Figure 2a−d), corresponding to the scheme shown in Figure 2e. In another example, Xu and co-workers successfully prepared the $MoSe_2$−$WSe_2$ monolayer lateral epitaxial hetero-nanostructures by the physical vapor transport mothed using $MoSe_2$ and $WSe_2$ powders as the precursors.[52] At the early stage of the growth process, it is favored to form pure $MoSe_2$ monolayer. However, after a certain time of growth, $WSe_2$ deposition dominates the growth, and the presence of $MoSe_2$ seed with active edges allows the further lateral epitaxial growth to form hetero-nanostructures. It is noted that pure $WSe_2$ crystals also grew during the process. It is worth emphasizing that no external action is required during the growth process, allowing for remaining the unpassivated edge sites for lateral epitaxy. Concurrently, Ajayan and co-workers developed a single-step vapor-phase growth process for preparation of highly crystalline lateral as well as vertically stacked $WS_2$−$MoS_2$ monolayer epitaxial hetero-structures.[53] It is believed that the sequential growth of $MoS_2$ and $WS_2$, instead of $Mo_xW_{1-x}S_2$ alloy, is due to the difference in nucleation and growth rates of $MoS_2$ and $WS_2$ crystals. When the reaction temperature was changed to about 850 °C, the $WS_2$ was epitaxially grown on the top of $MoS_2$ monolayer to form vertically stacked epitaxial hetero-nanostructures (Figure 3a−d). Surprisingly, when the reaction temperature was about 650 °C, the $WS_2$ preferred to further grow at the edge sites of the as-grown $MoS_2$ monolayer to form lateral epitaxial hetero-nanostructures (Figure 3e−h). Although the authors found that the addition of tellurium with tungsten powder can help to accelerate the melting of tungsten powder during the growth process, the essential role of tellurium in the formation of well-defined hetero-nanostructures needs to be further explored. Similarly, in a recent report, Jo and co-workers also demonstrated that tuning of the growth temperature is an effective approach for the nucleation kinetics control, thus to achieve the controlling of the growth mode of $MoS_2$−$WS_2$ hetero-nanostructures.[54] Cao and co-workers also reported the fabrication of vertical $MoS_2$−$WS_2$ hetero-nanostructures by a similar CVD method.[55] In another work, Lee and co-workers achieved the growth of lateral hetero-nanostructures of $MoS_2$−$WS_2$ and $MoSe_2$−$WSe_2$ monolayers by using ambient-pressure CVD with aromatic molecules as seeding promoters.[56] The growth process is similar to the


DOI: 10.1021/jacs.5b03590
J. Am. Chem. Soc. 2015, 137, 12162−12174

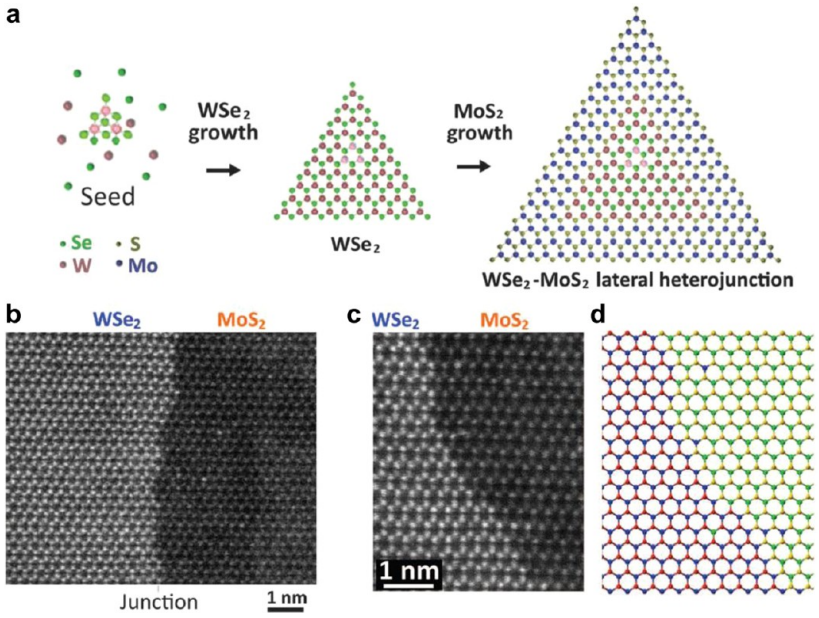


**Figure 4.** (a) Schematic illustration of the growth process of the monolayer $WSe_2$−$MoS_2$ lateral epitaxial hetero-structure. (b,c) High-resolution STEM images of the $WSe_2$−$MoS_2$ lateral epitaxial hetero-structure at the interface regions. (d) Atomic model showing the interface structure of the $WSe_2$−$MoS_2$ lateral epitaxial hetero-structure. Reproduced with permission from ref 58. Copyright 2015, American Association for the Advancement of Science.

method used by Xu and co-workers discussed above[52] except the use of perylene-3,4,9,10-tetracarboxylic acid tetrapotassium salt (PTAS) as seeding promoters. Very recently, Ajayan and co-workers reported the growth of vertical epitaxial $WSe_2$−$MoSe_2$ hetero-nanostructures by a two-step CVD method, which allows for finely controlling the domain size and the type of synthesized hetero-structures by simply tuning the growth time.[57] Note that alloyed structures are always observed at the interface regions for all the aforementioned monolayer lateral epitaxial hetero-nanostructures.[51−54,56] Importantly, recently, Li and co-workers developed a two-step CVD method to prepare monolayer $WSe_2$−$MoS_2$ lateral epitaxial hetero-nanostructure with an atomically sharp interface.[58] Monolayer $WSe_2$ was first grown on substrate via the VdW epitaxy. Then $MoS_2$ was epitaxially grown along the edge of $WSe_2$ seed in a separate finance (Figure 4a), the atomically sharp transition in compositions at the interface region was realized, which is evidenced by STEM images (Figure 4b−d).

Intriguingly, Geohegan and co-workers achieved the preparation of patterned arrays of monolayer $MoSe_2$−$MoS_2$ lateral epitaxial hetero-structures.[59] The monolayer $MoSe_2$ was first synthesized by CVD method and then simply masked by the conventional patterning processes (Figure 5a). The selective conversion of the unmasked $MoSe_2$ areas to $MoS_2$ was achieved by pulsed laser vaporization of sulfur (Figure 5a). Different shape of $MoS_2$ arrays, such as triangles, circles, and ribbons, can be prepared. For example, the Raman maps shown in Figure 5b clearly show the formation of triangular and circular $MoSe_2$ patterns on $MoS_2$ monolayer crystals. This strategy might be extended to prepare other kinds of patterned arrays of monolayer TMD lateral epitaxial hetero-nanostructures.

## LIQUID-PHASE EPITAXIAL GROWTH OF NANOSTRUCTURES ON 2D SEMICONDUCTOR NANOSHEETS

Note that all the aforementioned methods used for epitaxial growth of nanostructures on graphene or construction of TMD monolayer hetero-junctions belong to the gas-phase epitaxy technique. As known, the gas-phase epitaxy method normally requires high temperature/vacuum, and the prepared hetero-structures need to be supported by certain substrate, resulting in the high cost and relatively low output of the synthesis process.[7,8] In contrast, the liquid-phase epitaxial growth method allows for preparation of hetero-nanostructures in high yield and large amount with relatively low cost in solution phase.[9−15] The recent success in the high yield and massive preparation of semiconductor nanosheets in solution phase aroused great interest in utilization of them as dispersible templates for epitaxial growth of other nanostructures.[17−19] As a typical example, our group realized the epitaxial growth of noble metal nanocrystals including Pd, Pt, and Ag on dispersible single-layer $MoS_2$ nanosheets by wet-chemical methods at room temperature (Table 1).[60] The single-layer $MoS_2$ nanosheets that were used as the template for direct growth of noble metal nanostructures were prepared from its bulk crystal by an electrochemical Li intercalation and exfoliation method developed by our group.[61] For instance, the TEM image, selected area electron diffraction (SAED) pattern, and high-resolution TEM (HRTEM) image clearly show the successfully epitaxial deposition of Pd NPs with size of ∼5 nm on $MoS_2$ nanosheets (Figure 6a−c).[60] It was found that the Pd NPs show the major (111) and (101) orientation on the $MoS_2$(001) surface. The epitaxial deposition of Pt NPs with sizes of 1−3 nm on the $MoS_2$ monolayers was also achieved by the photochemical reduction, which is evidenced by the TEM image, SAED pattern, and HRTEM image (Figure 6e,f). In addition to the spherical NPs, Ag triangle nanoplates were also epitaxially grown on $MoS_2$ sheets, as shown in Figure 7a−c.


DOI: 10.1021/jacs.5b03590
J. Am. Chem. Soc. 2015, 137, 12162−12174

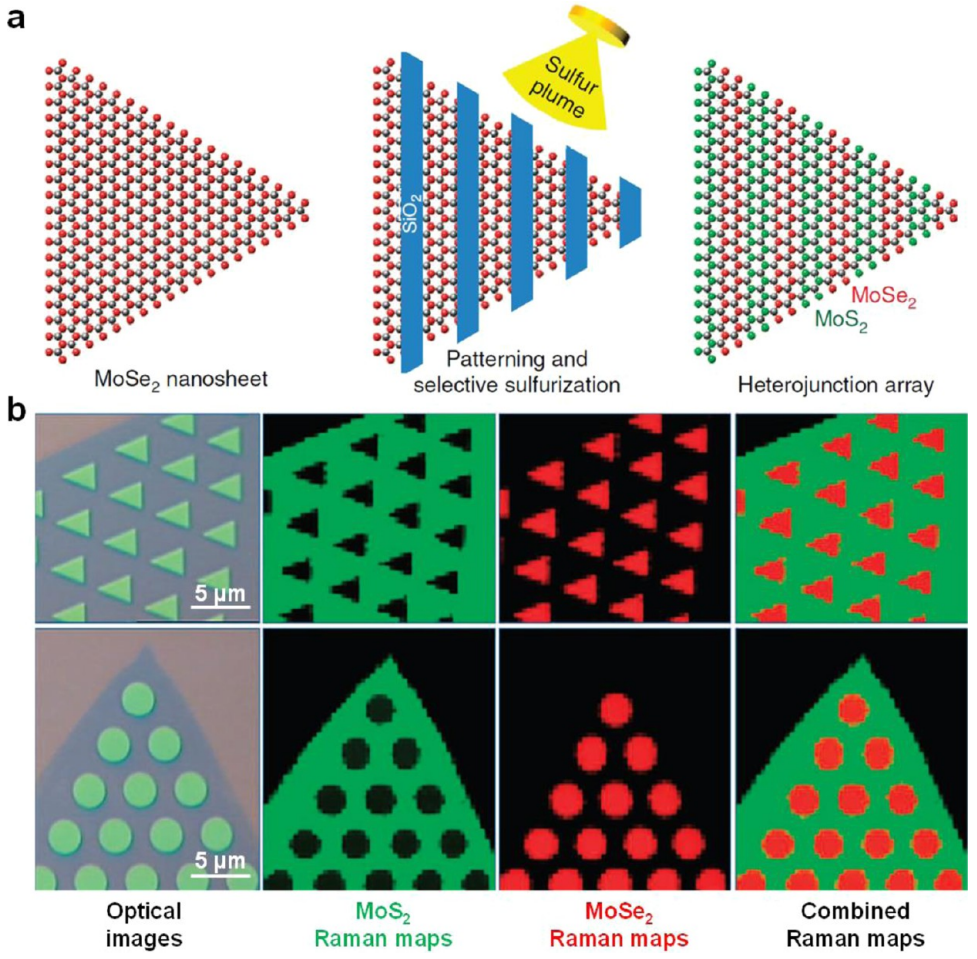


**Figure 5.** (a) Schematic illustration of the preparation process of $MoSe_2$–$MoS_2$ lateral epitaxial hetero-junction arrays. (b) Two examples of $MoSe_2$–$MoS_2$ lateral epitaxial hetero-junction arrays. The green, red, and combined Raman maps are obtained from the corresponding optical images, representing the $MoS_2$ (intensity map at 403 $cm^{-1}$), $MoSe_2$ (intensity map at 238 $cm^{-1}$), and overlaid $MoSe_2$–$MoS_2$ regions, respectively. Reproduced with permission from ref 59. Copyright 2015, Nature Publishing Group.

This is the first time to realize the epitaxial growth of noble metal nanocrystals on dispersible nanosheets in aqueous solution via wet chemical syntheses. Note that not all the noble metal nanocrystals are epitaxially aligned on the $MoS_2$ surface, in which the epitaxial ratio of Pt and Pd NPs is about 70%. The non-epitaxial growth of some NPs might be induced by the defects and edges in the single-layer $MoS_2$ sheets. It has been observed that there are some defects on the backbone of $MoS_2$ sheets, which might be generated by the Li-intercalation during the preparation of $MoS_2$ sheets. Since the epitaxial growth normally needs perfect crystal surface, the Pt or Pd NPs grown on the defects or edge sites belong to the non-epitaxial growth.

Besides noble metals, semiconductor nanostructures have also been successfully deposited on ultrathin 2D semiconductor nanosheets with epitaxial growth effect (Table 1).[62,63] For example, Zaumseil and co-workers reported the epitaxial growth of PbSe quantum dots (QDs) on $MoS_2$ or $WS_2$ nanoflakes by a wet-chemical method.[62] The $MoS_2$ and $WS_2$ nanoflakes were synthesized by ultrasonication of their bulk crystals in diphenyl ether with subsequent purification by centrifugation. The PbSe QDs were epitaxially grown on $MoS_2$ or $WS_2$ nanoflakes by using a hot-injection method from PbO and selenium powder in the presence of as-exfoliated $MoS_2$ or $WS_2$ nanoflakes. It is worth pointing out that the epitaxial ratio of PbSe QDs on $MoS_2$ or $WS_2$ nanoflakes is relatively low, which might be due to the defects on the nanoflake surface. Besides NPs, our group recently demonstrated the liquid-phase epitaxial growth of 2D semiconductor hetero-nanostructures by an electrochemical method,[63] which is similar to the Li intercalation and exfoliation method used for the high-yield and massive production of single- or few-layer TMD nanosheets from their bulk crystals.[61] As a result, ultrathin CuS nanoplates were epitaxially grown on $TiS_2$ nanosheets by using Cu foil and $TiS_2$ crystal as precursors. The obtained CuS nanoplates showed triangular/hexagonal shape with size of 50–120 nm (Figure 7d,e). Unlike the aforementioned epitaxial growth of NPs in liquid phase, all of the CuS nanoplates were perfectly aligned on the $TiS_2$ nanosheet without any misorientation (Figure 7f). This method is also applicable for epitaxial deposition of ZnS and $Ni_3S_2$ nanoplates on $TiS_2$ nanosheets by simply changing the metal foil. This is the first time for the realization of epitaxial growth of 2D semiconductor hetero-nanostructures in liquid phase.

## LIQUID-PHASE EPITAXIAL GROWTH OF CORE–SHELL NOBLE METAL NANOSHEETS

Besides graphene and TMD nanosheets, ultrathin 2D noble metal nanostructures are also receiving increasing attention recently.[25] To date, a number of ultrathin noble metal


DOI: 10.1021/jacs.5b03590
J. Am. Chem. Soc. 2015, 137, 12162–12174

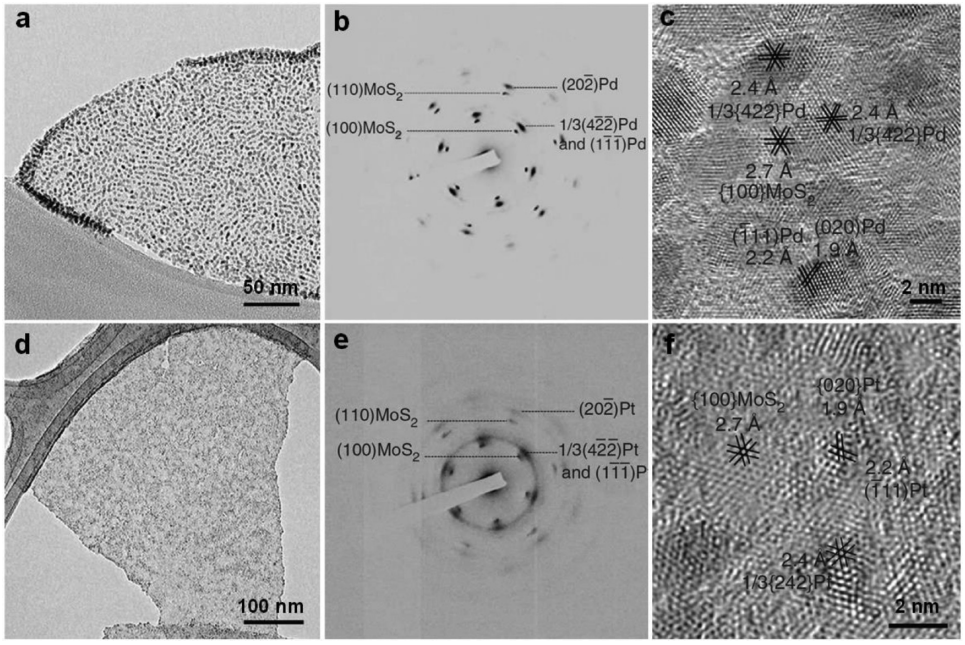


**Figure 6.** (a) TEM image of Pd NPs grown on $MoS_2$ nanosheet. (b) SAED pattern of a Pd−$MoS_2$ hybrid nanosheet. (c) HRTEM images of Pd NPs on $MoS_2$. (d) TEM image of Pt NPs grown on $MoS_2$ nanosheet. (e) SAED pattern of a Pt-$MoS_2$ hybrid nanosheet. (f) HRTEM images of Pt NPs on $MoS_2$. Reproduced with permission from ref 60. Copyright 2013, Nature Publishing Group.

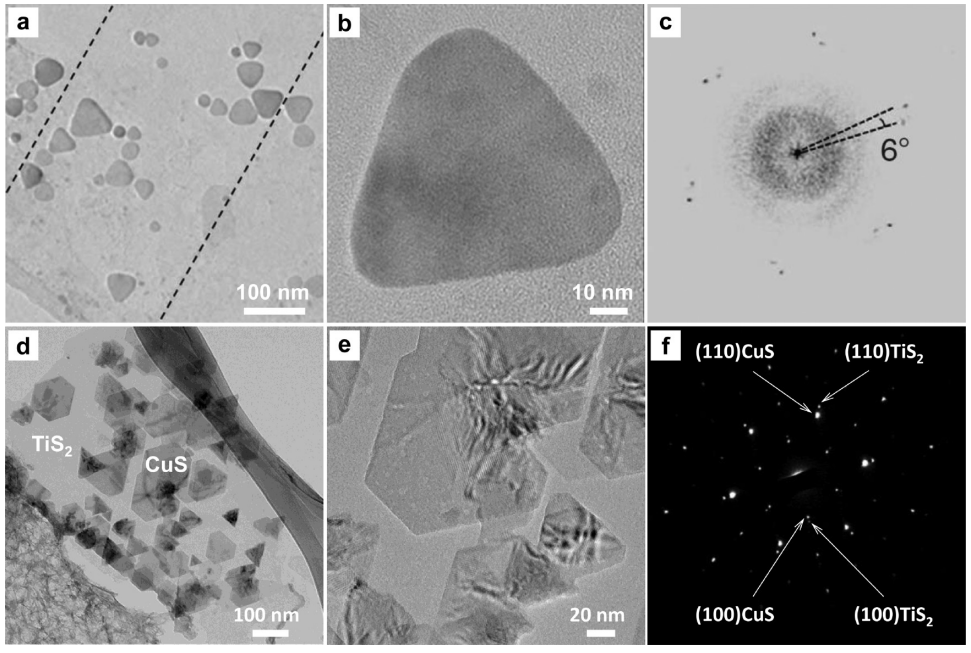


**Figure 7.** (a) TEM image of Ag nanoplates epitaxially grown on $MoS_2$ nanosheet. (b) TEM image of a typical Ag nanoplate epitaxially grown on $MoS_2$ nanosheet. (c) Fast Fourier transform (FFT)-generated SAED pattern of (b). Reproduced with permission from ref 60. Copyright 2013, Nature Publishing Group. (d) TEM image of epitaxial CuS−$TiS_2$ hetero-nanostructures. (e) Highly magnified TEM image of CuS−$TiS_2$ hetero-nanostructures. (f) The SAED pattern of epitaxial CuS−$TiS_2$ hetero-nanostructures. Reproduced with permission from ref 63. Copyright 2015, John Wiley & Sons, Inc.

nanosheets, such as Au, Pd, and Rh, have been synthesized by various methods, offering novel templates for epitaxial growth of hetero-nanostructures.[64−67] As a typical example, our group first synthesized ultrathin Au square sheets (AuSSs) with edge length of 200−500 nm and thickness of ∼2.4 nm on GO sheets.[67] Impressively, it was found that the crystalline AuSS is hexagonal close-packed (*hcp*) structure, which is stable under ambient conditions, rather than the conventional face-centered cubic (*fcc*) structure. By using this *hcp* AuSS as the template, a number of noble metal epitaxial core−shell hetero-nanostructures, such as Au@Ag, Au@Pt, and Au@Pd, were prepared (Table 1).[68,69] For example, Ag can be easily coated on the AuSSs via the reduction of $AgNO_3$ with L-ascorbic acid or $NaBH_4$ in the presence of the as-prepared AuSSs.[68] It is worth pointing out that a phase transformation of AuSSs from *hcp* to *fcc* structures was always observed during the formation of


DOI: 10.1021/jacs.5b03590
J. Am. Chem. Soc. 2015, 137, 12162−12174

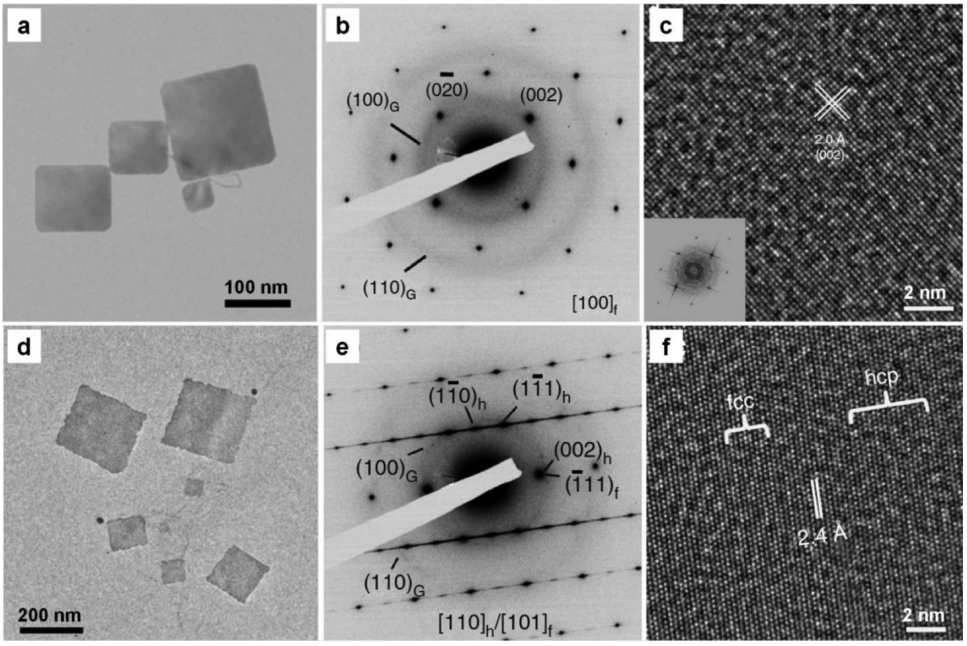


**Figure 8.** (a) TEM image of epitaxial *fcc* Au@Ag square nanosheets on GO surface. (b) SAED pattern of a typical epitaxial *fcc* Au@Ag square nanosheet taken along the $[100]_f$ zone axes. (c) HRTEM image of a typical epitaxial *fcc* Au@Ag square nanosheet. (d) TEM image of epitaxial *hcp*/*fcc* Au@Ag square nanosheets on GO surface. (e) SAED pattern of a typical epitaxial *hcp*/*fcc* Au@Ag square nanosheet along the $[110]_h/[101]_f$ zone axis. (f) HRTEM image of a typical epitaxial *hcp*/*fcc* Au@Ag square nanosheet. Reproduced with permission from ref 68. Copyright 2015, Nature Publishing Group.

epitaxial core−shell nanosheets. Note that Ag is favorable to epitaxially grow on Au surface due to the negligible lattice mismatch (~0.2%) between Au and Ag.[68] The resultant epitaxial core−shell Au@Ag nanosheets have a similar square shape with the AuSSs (Figure 8a). Its thickness could be tuned from 3 to 4.6 nm by controlling the amount of deposited Ag. The HRTEM image and SAED pattern revealed that the Au@Ag sheets is a pure *fcc* crystal structure with the $(100)_f$ orientation (Figure 8b,c). The epitaxial core−shell Au@Ag nanosheets can also be prepared by reduction of $AgNO_3$ with oleylamine.[68] In contrast to the pure *fcc* structure, the Au@Ag nanosheets prepared by using oleylamine as the reduction agent exhibited a crystal structure with the mixed *hcp*/*fcc* phase (Figure 8d−f). The thickness of the epitaxial *hcp*/*fcc* Au@Ag nanosheets is 2.8 ± 0.5 nm. It is suggested that the interplay of the surfactant−metal bonding energy and the adhesive energy of metal structures might be attributed to the different types of phase transformation induced by different capping agent. Similarly, the epitaxial growth of Pt or Pd on AuSSs to form the core−shell Au@Pt or Au@Pd nanoplates was achieved, in which the phase transformation from the *hcp* to *fcc* structures was also observed.[69] Unlike the epitaxial growth of Ag, the square shape of AuSSs changed to rhombic shape after the epitaxial growth Pt or Pd thin layer on its surface. Moreover, the epitaxial growth of Pt or Pd on *hcp* AuSSs mainly leads to the formation of *fcc* core−shell Au@Pt or Au@Pd rhombic nanoplates with $(101)_f$ orientation, which is much different from the $(100)_f$-orientated *fcc* Au@Ag nanosheets. The thickness of core−shell nanoplates is a little thicker than the pure *hcp* AuSSs. For example, the thickness of epitaxial Au@Pt rhombic nanoplates is about 3.5 ± 0.7 nm. Note that a little amount (<10%) of *fcc* $(100)_f$-oriented Au@Pt and Au@Pd square nanoplates were also obtained. We think the formation of unprecedented $(101)_f$-oriented nanoplates and the shape transformation are induced by the relatively large lattice mismatch between Pt or Pd and Au (e.g., 5.8% for Pt and 6.9% for Pd)[69] as compared to that between Ag and Au (0.2%).[68]

## UNIQUE ADVANTAGES OF EPITAXIAL HETERO-NANOSTRUCTURES BASED ON ULTRATHIN 2D NANOSHEETS

Previous studies have demonstrated that engineering hybrid nanomaterials or hetero-nanostructures based on ultrathin 2D nanosheets, such as graphene and TMDs, could be one of the most simple and effective ways to tune their physical, chemical, and/or electronic properties and thus to fully exploit their various promising applications.[28−30] Epitaxial hetero-nanostructures, as one kind of hetero-nanostructures, are believed to be promising candidates for some specific applications due to their well-defined structure/interface and selectively exposed facets enabled by the epitaxial growth nature. Especially, the epitaxial growth of hetero-nanostructures enables them with some advantages that are unattainable with the other forms of hetero-nanostructures. In this section, the potential of the as-prepared epitaxial hetero-nanostructures based on ultrathin 2D nanosheets used for some applications will be discussed.

Ultrathin 2D nanosheets, especially graphene and TMDs, have shown potential in the fabrication of electronic/optoelectronic devices, such as transistors, phototransistors, nanogenerators, and electrical gas sensors.[31,38−41] The creation of p−n junctions with well-defined structures is fundamentally important in all modern electronics/optoelectronics, such as p−n diodes, photovoltaic devices, and light-emitting diodes (LEDs). The construction of epitaxial hetero-nanostructures based on ultrathin 2D nanosheets could be a promising platform to engineer their electronic properties, opening up new ways to create fascinating hetero-junctions at atomic/nanometer scale. As a typical example, Duan and co-workers


DOI: 10.1021/jacs.5b03590
J. Am. Chem. Soc. 2015, 137, 12162−12174

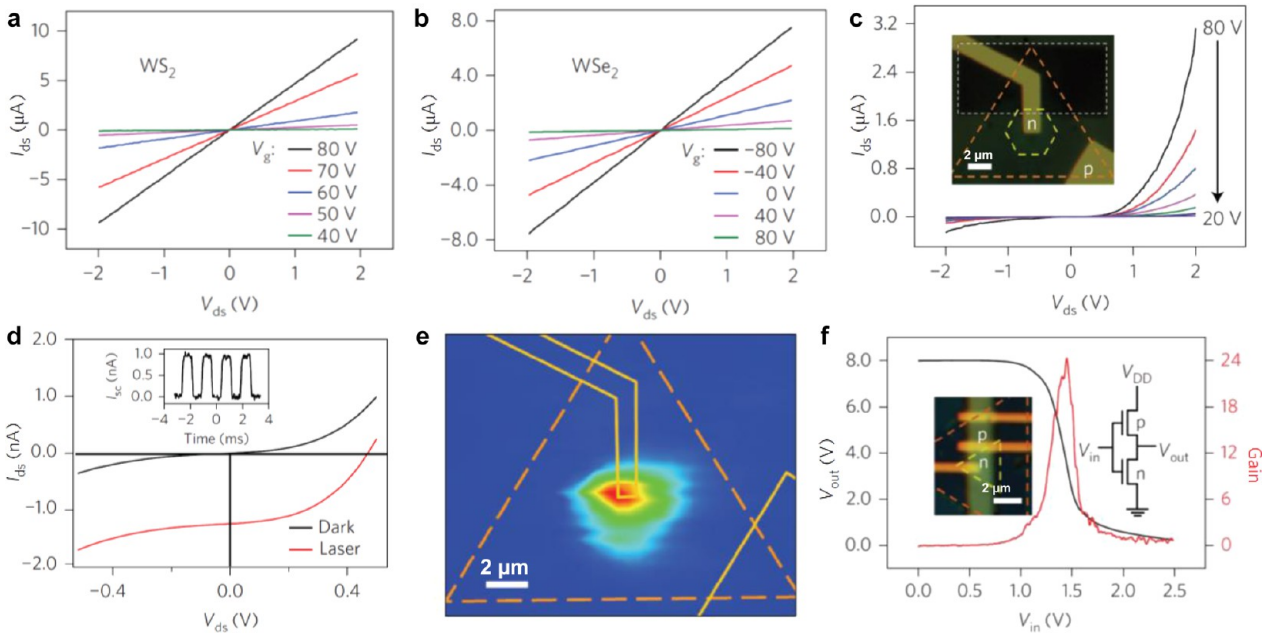


**Figure 9.** (a) $I_{ds}$–$V_{ds}$ output characteristics of an n-type $WS_2$ FET at various backgate voltages. (b) $I_{ds}$–$V_{ds}$ output characteristics of a p-type $WSe_2$ FET at various backgate voltages. (c) Gate-tunable output characteristics of a lateral $WSe_2$–$WS_2$ hetero-junction p–n diode. (d) Experimental output ($I_{ds}$–$V_{ds}$) characteristics of the lateral $WSe_2$–$WS_2$ hetero-junction p–n diode in the dark and under illumination. Inset: Temporal photocurrent response under periodic on/off laser illumination through a mechanical chopper. (e) Scanning photocurrent mapping image of the lateral $WSe_2$–$WS_2$ hetero-junction p–n diode. (f) A CMOS inverter obtained by integrating a p-type $WSe_2$ and n-type $WS_2$ FET. Inset: Image and circuit diagram of the $WSe_2$–$WS_2$ CMOS inverter. Reproduced with permission from ref 51. Copyright 2014, Nature Publishing Group.

demonstrated that the $WSe_2$–$WS_2$ lateral epitaxial hetero-nanostructure could be used for many functional devices, including photodiodes and complementary metal oxide–semiconductor (CMOS) inverters (Figure 9).[51] Note that the $WSe_2$–$WS_2$ lateral hetero-nanostructure is a p–n junction, since the $WSe_2$ is a p-type semiconductor and $WS_2$ is an n-type semiconductor, which are confirmed by their field emission transistor properties (Figure 9a,b). The formation of p–n diode was also evidenced by the current rectification of the device fabricated with the $WSe_2$–$WS_2$ lateral hetero-nanostructure (Figure 9c). The photocurrent response of the photodiode based on $WSe_2$–$WS_2$ p–n junction was investigated, and a photovoltaic effect with an open-circuit voltage of ∼0.47 V and a short-circuit current of ∼1.2 nA was observed (Figure 9d). The response time of the device is less than 100 $\mu$s, which is beyond the experimental resolution, indicating that the photoresponse comes from the photocarrier generation and separation. The calculated external quantum efficiency of photon-to-electron conversion of the $WSe_2$–$WS_2$ p–n photodiode is about ∼9.9%, while the internal quantum efficiency of the photodiode is estimated to be as high as 43%. The photoluminescence mapping revealed that the photocurrent response is localized to the lightly doped $WS_2$ and $WSe_2$–$WS_2$ interface region (Figure 9e), indicating that the depletion layer is dominated by the lightly doped $WS_2$ layer. Besides photodiode, by integrating a p-channel $WSe_2$ and an n-channel $WS_2$ transistor in series across the hetero-junction interface, the $WSe_2$–$WS_2$ p–n junction could also be used for construction of a CMOS inverter (a logic NOT gate). A 20 nm $HfO_2$ thin film was used as the gate dielectric in the CMOS inverter to reduce the required gate voltage. Constant high voltage output at low input was detected on this device based on its output–input ($V_{out}$–$V_{in}$) voltage response (Figure 9f). The output voltage was quickly switched to nearly 0 V and maintained at a low state at higher input voltages when the input voltage increased to ∼1.5 V. Importantly, a voltage gain as large as 24 on the CMOS inverter was achieved, which was revealed by the differentiation of measured $V_{out}$–$V_{in}$ relation. Such a large gain is of significance for the interconnection of arrays of logic circuits for functional electronic applications, in which the signal restoration at each stage is not necessary. Similarly, Ajayan and co-workers also demonstrated the lateral $WS_2$–$MoS_2$ hetero-nanostructure, being an intrinsic monolayer p–n junction without external electrical tuning, was used as the photodiode.[53] A photovoltaic effect was observed on the photodiode with an open-circuit voltage of 0.12 V and closed-circuit current of 5.7 pA, which is not as good as the photodiode based on the lateral $WSe_2$–$WS_2$ hetero-nanostructure.[51]

Besides the lateral epitaxial hetero-nanostructure, Ajayan and co-workers also demonstrated that the $WS_2$–$MoS_2$ vertical epitaxial hetero-nanostructure could be a promising channel material for integration of high performance field-effect transistors (FETs).[53] It was demonstrated that the ON/OFF ratio of the FET device based on the $WS_2$–$MoS_2$ vertical epitaxial hetero-nanostructure is larger than $10^6$. Its mobility is estimated to be in the range of 15–34 $cm^2\ V^{-1}\ s^{-1}$, which is much higher compared to the monolayer $MoS_2$ (4.5 $cm^2\ V^{-1}\ s^{-1}$)[70,71] or $MoS_2$ bilayer (5.7 $cm^2\ V^{-1}\ s^{-1}$).[53] More importantly, the mobility is much higher than that of the VdW $WS_2$–$MoS_2$ hetero-structure made by the transfer method (0.51 $cm^2\ V^{-1}\ s^{-1}$).[53] It is suggested that the excellent device performance of the epitaxial hetero-structures is ascribed to the clean interface between $WS_2$ and $MoS_2$. In contrast, unwanted contaminations, which were introduced during the transfer process, might exist between the stacking $WS_2$ and $MoS_2$ layer, resulting in the relatively poor performance of the FET device.[53]



DOI: 10.1021/jacs.5b03590
J. Am. Chem. Soc. 2015, 137, 12162–12174

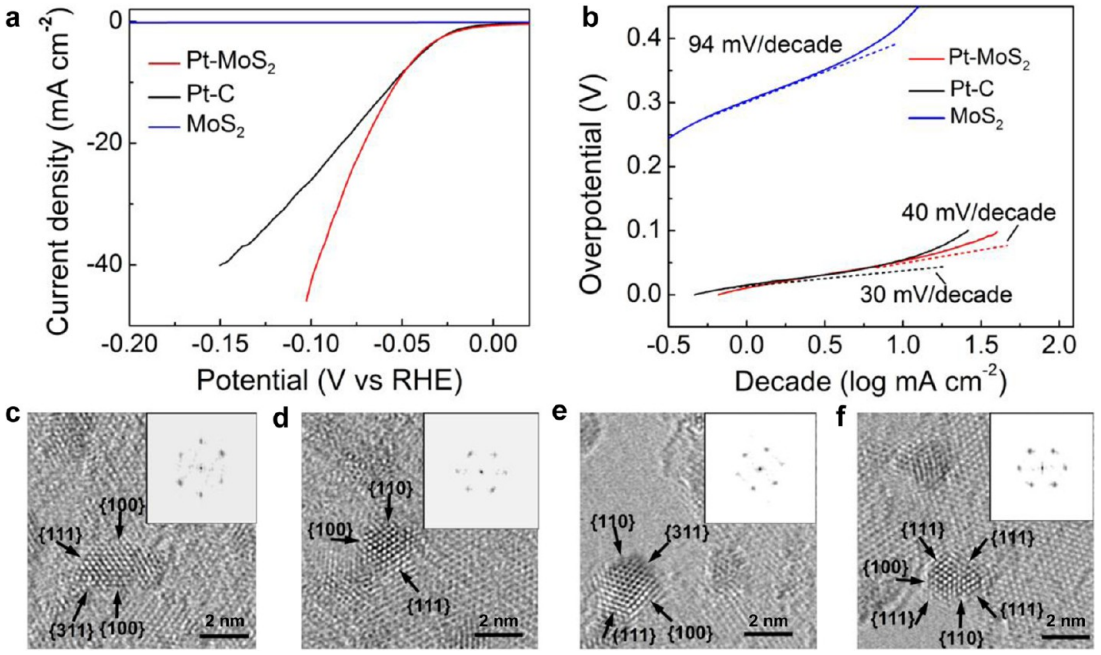


**Figure 10.** (a) Polarization curves of Pt−$MoS_2$, Pt−C, and $MoS_2$. (b) The corresponding Tafel plots. (c−f) HRTEM images of (101)-oriented Pt NPs on $MoS_2$. Reproduced with permission from ref 60. Copyright 2013, Nature Publishing Group.

Recently, Robinson and co-workers demonstrated that the $MoS_2$ nanosheets epitaxially grown on graphene presented much improved photoconductivity and responsivity compared to the pure $MoS_2$ nanosheet when used as the channel material in phototransistors.[35] It was found that photocurrent of the phototransistor based on $MoS_2$−graphene hetero-nanostructure is more than 100 times higher than that of the single-layer $MoS_2$ phototransistor. Its photoresponsivity is about 40 $mAW^{-1}$, which is much higher than that of the $MoS_2$ phototransistor (0.42 $mAW^{-1}$).[39] In addition, Zaumseil and co-workers reported that photodetector could be constructed based on the solution-processed PbSe QD-deposited $MoS_2$ flakes.[62] The obtained photodetector with a near-infrared photosensitivity exhibited much enhanced photocurrent compared to the pure $MoS_2$ nanosheet. Importantly, this device exhibited long-term stability in air, and no obvious degradation was observed even after 48 cycles. However, the curial role of epitaxial growth in this device was not discussed, which should be further explored.

It is well known that Pt is a highly efficient catalyst for some electrocatalytic reactions, such as hydrogen evolution reaction (HER) and oxygen reduction reaction (ORR).[72] The exposed crystal facet of Pt nanocrystal is one of key factors that can affect its catalytic activity, in which the high-index facet normally exhibits higher catalytic activity compared to the low-index facet.[73] Hetero-nanostructures by epitaxial growth of noble metal nanocrystals on 2D well-defined crystalline surface could be used as high efficient catalysts for electrocatalysis. Recently, our group demonstrated that the composite of Pt NPs epitaxially grown on single-layer $MoS_2$ nanosheets, referred to as Pt−$MoS_2$, could be a highly efficient catalyst for HER.[60] It was found that the Pt−$MoS_2$ composite exhibited much higher electrocatalytic activity toward the HER compared with the pure $MoS_2$ nanosheets as well as the commercial Pt−C catalyst with the same Pt loading (Figure 10a). The calculated Tafel slopes of for the three tested catalysts are shown in Figure 10b. The enhanced electrocatalytic activity toward HER could be partially attributed to the epitaxially grown Pt NPs with exposed high index facets, since some high index facets such as {110} and {311} were observed in the Pt NPs synthesized on $MoS_2$ (Figure 10c-f). Moreover, the large surface area of 2D $MoS_2$ nanosheets makes it easy to collect and transport charges, which is beneficial to the efficient charge transfer and ionic interchange at the catalyst surface.

## ■ CONCLUSION AND PROSPECTS

In summary, ultrathin 2D nanosheets with some interesting properties could serve as new, fascinating platforms for engineering well-defined hetero-nanostructures at the atomic/nanometer scale. In particular, ultrathin 2D nanosheets with atomically flat surfaces show promise for use as templates for epitaxial deposition of other nanostructures on their surfaces. Noble metal, semiconductor, and topological insulator nanostructures have been successfully epitaxially grown on graphene, $MoS_2$, or $TiS_2$ nanosheets.[32−36,60,62,63] In addition, the liquid-phase epitaxial growth of noble metal core−shell nanosheets (e.g., Au@Ag, Au@Pt, and Au@Pd) has also been achieved by using *hcp* AuSSs as template.[68,69] Moreover, the lateral and vertical epitaxial hetero-nanostructures can be constructed by epitaxial growth of one kind of TMD monolayer at the edge or on the top of an existing TMD monolayer. 2D lateral or vertical epitaxial TMD hetero-nanostructures, such as $MoSe_2$−$MoS_2$, $WSe_2$−$WS_2$, $MoSe_2$−$WSe_2$, $WS_2$−$MoS_2$, and $WSe_2$−$MoS_2$, have been achieved by using gas-phase epitaxy methods.[51−59] The epitaxial growth enabled them some advantages, offering them much potential for some specific applications. For example, the seamless lateral epitaxial TMD hetero-nanostructure formed via the covalent bond is one kind of p−n junctions, allowing for the integration of many functional electronic devices by using it as the basic unit, such as transistors, photodiodes, LEDs, and photovoltaic devices.[50,51] The clean and well-defined interface of vertical epitaxial TMD hetero-nanostructures makes them ideal platforms for construction of high-performance electronics and


DOI: 10.1021/jacs.5b03590
J. Am. Chem. Soc. 2015, 137, 12162−12174

optoelectronics.[53] Furthermore, epitaxially grown noble metal nanostructures on 2D nanosheets with selectively exposed facets could be excellent catalysts in some electrocatalytic reactions (e.g., HER).[60]

Despite all the recent achievements in this exciting research area, challenges still remain in the highly controlled synthesis of epitaxial hetero-nanostructures and understanding of the underlying mechanisms. Although 2D epitaxial hetero-nanostructures have shown some advances, the realization of such advances relies on the epitaxial growth of hetero-nanostructures based on ultrathin 2D nanosheets in a highly controlled manner. For example, all the reported lateral TMD epitaxial hetero-nanostructures are based on the formation of an inside monolayer surrounded by an outside lateral layer. However, electrode fabrication on such kinds of hetero-nanostructures is more difficult compared to that on the normal hetero-structures. One of the greatest challenges lies in how we can achieve controlled synthesis of epitaxial hetero-nanostructures based on ultrathin 2D nanosheets with desired composition, orientation, interconnection manner, and surface exposure. Moreover, although some epitaxial hetero-nanostructures based on ultrathin 2D nanosheets have been prepared, the intrinsic mechanisms underlying the formation of such kinds of epitaxial hetero-nanostructures are rarely studied. Understanding the mechanisms behind the epitaxial growth process is of importance in order to guide the further epitaxial growth of hetero-nanostructures based on ultrathin 2D nanosheets at a highly controllable level. In addition, finding effective techniques for investigation of the growth mechanisms for these epitaxial hetero-nanostructures is another challenge.

The epitaxial growth of hetero-nanostructures based on ultrathin 2D nanosheets is still in its infancy, but the advances arising from the epitaxial growth on these hetero-nanostructures will inspire increasing research in this promising field. Beyond the currently used 2D nanosheets, such as graphene, noble metals, and some TMD nanosheets (e.g., $MoS_2$, $WS_2$, $MoSe_2$, and $WSe_2$), there are many other ultrathin 2D nanosheets with varying physical and electronic properties, such as other TMDs (e.g., $TaS_2$, $HfS_2$, $TiSe_2$, $NbS_2$, $VSe_2$, and $WTe_2$),[17] h-BN,[19,20] metal oxides,[20] and black phosphorus.[66] Moreover, many other 2D nanomaterials, such as metal−organic frameworks (MOFs),[74] covalent−organic frameworks (COFs),[75] and organic crystals,[76−79] have also been prepared in the past few years. Some epitaxial hetero-nanostructures could be constructed on the basis of these new ultrathin 2D nanosheets. For example, 2D MOF-based epitaxial hetero-nanostructures could be prepared by epitaxial growth of single- or few-layer MOF nanosheets on graphene or monolayer $MoS_2$. It is believed that the epitaxial hetero-nanostructures based on these 2D nanostructures, especially MOFs, COFs, and organic crystals, may have some properties and advanced functions due to their epitaxial nature. Moreover, some specific techniques are required for studying the mechanism underlying the epitaxial growth process. For example, in situ TEM and X-ray photoelectron spectroscopy (XPS) could be useful to monitor the whole epitaxial growth process, which is helpful for investigation of the growth mechanisms. In addition, theoretical calculations can be carried out to gain a deeper understanding of the mechanism together with the experimental results.

Although some epitaxial hetero-nanostructures have exhibited excellent performance in specific applications, many other epitaxial hetero-nanostructures still need to be explored. For example, the advantages of epitaxial noble metal core−shell nanosheets and topological insulator nanoplates epitaxially grown on graphene have not been explored. Epitaxial core−shell Au@Pt nanosheets[69] may have excellent catalytic activities for some catalytic reactions. Moreover, hetero-nanostructures formed by epitaxial growth of 2D MOFs or organic crystals on graphene or TMD nanosheets could be promising candidates for construction of high-performance functional optoelectronic devices, such as p−n diodes, photovoltaic devices, and LEDs. Therefore, more efforts are expected to be devoted to the exploration of the advantages of other epitaxial hetero-nanostructures in the near future.

## AUTHOR INFORMATION


### Corresponding Author

*hzhang@ntu.edu.sg


### Notes

The authors declare no competing financial interest.

## ACKNOWLEDGMENTS

This work was supported by the Ministry of Education under AcRF Tier 2 (ARC 26/13, No. MOE2013-T2-1-034), AcRF Tier 1 (RGT18/13 and RG5/13), Start-Up Grant (M4080865.070.706022), and Singapore Millennium Foundation in Singapore. This Research is also conducted by NTU-HUJ-BGU Nanomaterials for Energy and Water Management Programme under the Campus for Research Excellence and Technological Enterprise (CREATE), that is supported by the National Research Foundation, Prime Minister's Office, Singapore.

## REFERENCES


(1) Matthews, J. W. *Epitaxial growth*; Matthews, J. W., Ed.; Academic Press: New York, 1975.
(2) Harada, Y.; Ozaki, H.; Ohno, K. *Phys. Rev. Lett.* **1984**, *52*, 2269.
(3) DeRose, J. A.; Thundat, T.; Nagahara, L. A.; Lindsay, S. M. *Surf. Sci.* **1991**, *256*, 102−108.
(4) Yamada, I.; Inokawa, H.; Takagi, T. *J. Appl. Phys.* **1984**, *56*, 2746.
(5) Voigtländer, B.; Meyer, G.; Amer, N. M. *Phys. Rev. B: Condens. Matter Mater. Phys.* **1991**, *44*, 10354.
(6) Costi, R.; Saunders, A. E.; Banin, U. *Angew. Chem., Int. Ed.* **2010**, *49*, 4878−4897.
(7) Nagpal, P.; Lindquist, N. C.; Oh, S. H.; Norris, D. J. *Science* **2009**, *325*, 594−597.
(8) Komanicky, V.; Iddir, H.; Chang, K. C.; Menzel, A.; Karapetrov, G.; Hennessy, D.; Zapol, P.; You, H. *J. Am. Chem. Soc.* **2009**, *131*, 5732−5733.
(9) Peng, X. G.; Schlamp, M. C.; Kadavanich, A. V.; Alivisatos, A. P. *J. Am. Chem. Soc.* **1997**, *119*, 7019−7029.
(10) Habas, S. E.; Lee, H.; Radmilovic, V.; Somorjai, G. A.; Yang, P. D. *Nat. Mater.* **2007**, *6*, 692−697.
(11) Xue, C.; Millstone, J. E.; Li, S.; Mirkin, C. A. *Angew. Chem., Int. Ed.* **2007**, *46*, 8436−8439.
(12) Lu, C. L.; Prasad, K. S.; Wu, H. L.; Ho, J. A. A.; Huang, M. H. *J. Am. Chem. Soc.* **2010**, *132*, 14546−14553.
(13) Seo, D.; Yoo, C. I.; Jung, J.; Song, H. *J. Am. Chem. Soc.* **2008**, *130*, 2940−2941.
(14) Sun, X. L.; Guo, S. J.; Liu, Y.; Sun, S. H. *Nano Lett.* **2012**, *12*, 4859−4863.
(15) Wang, W. S.; Goebl, J.; He, L.; Aloni, S.; Hu, Y. X.; Zhen, L.; Yin, Y. D. *J. Am. Chem. Soc.* **2010**, *132*, 17316−17324.
(16) Geim, A. K.; Novoselov, K. S. *Nat. Mater.* **2007**, *6*, 183−191.
(17) Chhowalla, M.; Shin, H. S.; Eda, G.; Li, L. J.; Loh, K.; Zhang, H. *Nat. Chem.* **2013**, *5*, 263−275.
(18) Huang, X.; Zeng, Z. Y.; Zhang, H. *Chem. Soc. Rev.* **2013**, *42*, 1934−1946.




DOI: 10.1021/jacs.5b03590
*J. Am. Chem. Soc.* 2015, 137, 12162−12174

(19) Nicolosi, V.; Chhowalla, M.; Kanatzidis, M. G.; Strano, M. S.; Coleman, J. N. *Science* **2013**, *340*, 1226419.
(20) Xu, M. S.; Liang, T.; Shi, M. M.; Chen, H. Z. *Chem. Rev.* **2013**, *113*, 3766−3798.
(21) Allen, M. J.; Tung, V. C.; Kaner, R. B. *Chem. Rev.* **2010**, *110*, 132−145.
(22) Wang, Q. H.; Kalantar-Zadeh, K.; Kis, A.; Coleman, J. N.; Strano, M. S. *Nat. Nanotechnol.* **2012**, *7*, 699−712.
(23) Sun, Y. F.; Gao, S.; Xie, Y. *Chem. Soc. Rev.* **2014**, *43*, 530−546.
(24) Chen, Y.; Tan, C. L.; Zhang, H.; Wang, L. Z. *Chem. Soc. Rev.* **2015**, *44*, 2681−2701.
(25) Fan, Z. X.; Huang, X.; Tan, C. L.; Zhang, H. *Chem. Sci.* **2015**, *6*, 95−111.
(26) Tan, C. L.; Zhang, H. *Nat. Commun.* **2015**, *6*, 7873.
(27) Tan, C. L.; Yu, P.; Hu, Y. L.; Chen, J. Z.; Huang, Y.; Cai, Y. Q.; Luo, Z. M.; Li, B.; Lu, Q. P.; Wang, L. H.; Liu, Z.; Zhang, H. *J. Am. Chem. Soc.* **2015**, *137*, 10430−10436.
(28) Huang, X.; Qi, X. Y.; Boey, F.; Zhang, H. *Chem. Soc. Rev.* **2012**, *41*, 666−686.
(29) Huang, X.; Tan, C. L.; Yin, Z. Y.; Zhang, H. *Adv. Mater.* **2014**, *26*, 2185−2204.
(30) Tan, C. L.; Zhang, H. *Chem. Soc. Rev.* **2015**, *44*, 2713−2731.
(31) Novoselov, K. S.; Geim, A. K.; Morozov, S. V.; Jiang, D.; Zhang, Y.; Dubonos, S. V.; Grigorieva, I. V.; Firsov, A. A. *Science* **2004**, *306*, 666−669.
(32) Dang, W. H.; Peng, H. L.; Li, H.; Wang, P.; Liu, Z. F. *Nano Lett.* **2010**, *10*, 2870−2876.
(33) Lin, M.; Wu, D.; Zhou, Y.; Huang, W.; Jiang, W.; Zheng, W. S.; Zhao, S. L.; Jin, C. H.; Guo, Y. F.; Peng, H. L.; Liu, Z. F. *J. Am. Chem. Soc.* **2013**, *135*, 13274−13277.
(34) Shi, Y. M.; Zhou, W.; Lu, A. Y.; Fang, W. J.; Lee, Y. H.; Hsu, A. L.; Kim, S. M.; Kim, K. K.; Yang, H. Y.; Li, L.-J.; Idrobo, J.-C.; Kong, J. *Nano Lett.* **2012**, *12*, 2784−2791.
(35) Lin, Y. C.; Lu, N.; Perea-Lopez, N.; Li, J.; Lin, Z.; Peng, X.; Lee, C. H.; Sun, C.; Calderin, L.; Browning, P. N.; Bresnehan, M. S.; Kim, M. J.; Mayer, T. S.; Terrones, M.; Robinson, J. A. *ACS Nano* **2014**, *8*, 3715−3723.
(36) Azizi, A.; Eichfeld, S.; Geschwind, G.; Zhang, K.; Jiang, B.; Mukherjee, D.; Hossain, L.; Piasecki, A. F.; Kabius, B.; Robinson, J. A.; Alem, N. *ACS Nano* **2015**, *9*, 4882−4890.
(37) Dreyer, D. R.; Park, S.; Bielawski, C. W.; Ruoff, R. S. *Chem. Soc. Rev.* **2010**, *39*, 228−240.
(38) Radisavljevic, B.; Radenovic, A.; Brivio, J.; Giacometti, V.; Kis, A. *Nat. Nanotechnol.* **2011**, *6*, 147−150.
(39) Yin, Z. Y.; Li, H.; Li, H.; Jiang, L.; Shi, Y. M.; Sun, Y. H.; Lu, G.; Zhang, Q.; Chen, X. D.; Zhang, H. *ACS Nano* **2012**, *6*, 74−80.
(40) Wu, W. Z.; Wang, L.; Li, Y. L.; Zhang, F.; Lin, L.; Niu, S. M.; Chenet, D.; Zhang, X.; Hao, Y. F.; Heinz, T. F.; Hone, J.; Wang, Z. L. *Nature* **2014**, *514*, 470−474.
(41) Li, H.; Yin, Z. Y.; He, Q. Y.; Li, H.; Huang, X.; Lu, G.; Fam, D. W. H.; Tok, A. I. Y.; Zhang, Q.; Zhang, H. *Small* **2012**, *8*, 63−67.
(42) Geim, A. K.; Grigorieva, I. V. *Nature* **2013**, *499*, 419−425.
(43) Georgiou, T.; Jalil, R.; Belle, B. D.; Britnell, L.; Gorbachev, R. V.; Morozov, S. V.; Kim, Y.-J.; Gholinia, A.; Haigh, S. J.; Makarovsky, O.; Eaves, L.; Ponomarenko, L. A.; Geim, A. K.; Novoselov, K. S.; Mishchenko, A. *Nat. Nanotechnol.* **2012**, *8*, 100−103.
(44) Pospischil, A.; Furchi, M. M.; Mueller, T. *Nat. Nanotechnol.* **2014**, *9*, 257−261.
(45) Baugher, B. W. H.; Churchill, H. O. H.; Yang, Y. F.; Jarillo-Herrero, P. *Nat. Nanotechnol.* **2014**, *9*, 262−267.
(46) Ross, J. S.; Klement, P.; Jones, A. M.; Ghimire, N. J.; Yan, J. Q.; Mandrus, D. G.; Taniguchi, T.; Watanabe, K.; Kitamura, K.; Yao, W.; Cobden, D. H.; Xu, X. D. *Nat. Nanotechnol.* **2014**, *9*, 268−272.
(47) Lim, H.; Yoon, S. I.; Kim, G.; Jang, A.-R.; Shin, H. S. *Chem. Mater.* **2014**, *26*, 4891−4903.
(48) Ji, Q. Q.; Zhang, Y.; Zhang, Y. F.; Liu, Z. F. *Chem. Soc. Rev.* **2015**, *44*, 2587−2602.
(49) Shi, Y. M.; Li, H. N.; Li, L.-J. *Chem. Soc. Rev.* **2015**, *44*, 2744−2756.
(50) Duesberg, G. S. *Nat. Mater.* **2014**, *13*, 1075−1076.
(51) Duan, X. D.; Wang, C.; Shaw, J. C.; Cheng, R.; Chen, Y.; Li, H. H.; Wu, X. P.; Tang, Y.; Zhang, Q. L.; Pan, A. L.; Jiang, J. H.; Yu, R. Q.; Huang, Y.; Duan, X. F. *Nat. Nanotechnol.* **2014**, *9*, 1024−1030.
(52) Huang, C. M.; Wu, S. F.; Sanchez, A. M.; Peters, J. J. P.; Beanland, R.; Ross, J. S.; Rivera, P.; Yao, W.; Cobden, D. H.; Xu, X. D. *Nat. Mater.* **2014**, *13*, 1096−1101.
(53) Gong, Y. J.; Lin, J. H.; Wang, X. L.; Shi, G.; Lei, S. D.; Lin, Z.; Zou, X. L.; Ye, G. L.; Vajtai, R.; Yakobson, B. I.; Terrones, H.; Terrones, M.; Tay, B. K.; Lou, J.; Pantelides, S. T.; Liu, Z.; Zhou, W.; Ajayan, P. M. *Nat. Mater.* **2014**, *13*, 1135−1142.
(54) Heo, H.; Sung, J. H.; Jin, G.; Ahn, J.-H.; Kim, K.; Lee, M.-J.; Cha, S.; Choi, H.; Jo, M.-H. *Adv. Mater.* **2015**, *27*, 3803−3810.
(55) Yu, Y. F.; Hu, S.; Su, L. Q.; Huang, L. J.; Liu, Y.; Jin, Z. H.; Purezky, A. A.; Geohegan, D. B.; Kim, K. W.; Zhang, Y.; Cao, L. Y. *Nano Lett.* **2015**, *15*, 486−491.
(56) Zhang, X. Q.; Lin, C.-H.; Tseng, Y.-W.; Huang, K.-H.; Lee, Y.-H. *Nano Lett.* **2015**, *15*, 410−415.
(57) Gong, Y.; Lei, S.; Ye, G.; Li, B.; He, Y.; Keyshar, K.; Zhang, X.; Wang, Q.; Lou, J.; Liu, Z.; Vajtai, R.; Zhou, W.; Ajayan, P. M. *Nano Lett.* **2015**, *15*, 6135−6141.
(58) Li, M.-Y.; Shi, Y.; Cheng, C.-C.; Lu, L.-S.; Lin, Y.-C.; Tang, H.-L.; Tsai, M.-L.; Chu, C.-W.; Wei, K.-H.; He, J.-H.; Chang, W.-H.; Suenaga, K.; Li, L.-J. *Science* **2015**, *349*, 524−528.
(59) Mahjouri-Samani, M.; Lin, M.-W.; Wang, K.; Lupini, A. R.; Lee, J.; Basile, L.; Boulesbaa, A.; Rouleau, C. M.; Puretzky, A. A.; Ivanov, I. N.; Xiao, K.; Yoon, M.; Geohegan, D. B. *Nat. Commun.* **2015**, *6*, 7749.
(60) Huang, X.; Zeng, Z. Y.; Bao, S. Y.; Wang, M. F.; Qi, X. Y.; Fan, Z. X.; Zhang, H. *Nat. Commun.* **2013**, *4*, 1444.
(61) Zeng, Z. Y.; Yin, Z. Y.; Huang, X.; Li, H.; He, Q. Y.; Lu, G.; Boey, F.; Zhang, H. *Angew. Chem., Int. Ed.* **2011**, *50*, 11093−11097.
(62) Schornbaum, J.; Winter, B.; Schießl, S. P.; Gannott, F.; Katsukis, G.; Guldi, D. M.; Spiecker, E.; Zaumseil, J. *Adv. Funct. Mater.* **2014**, *24*, 5798−5806.
(63) Tan, C. L.; Zeng, Z. Y.; Huang, X.; Rui, X. H.; Wu, X. J.; Li, B.; Luo, Z. M.; Chen, J. Z.; Chen, B.; Yan, Q. Y.; Zhang, H. *Angew. Chem., Int. Ed.* **2015**, *54*, 1841−1845.
(64) Duan, H. H.; Yan, N.; Yu, R.; Chang, C. R.; Zhou, G.; Hu, H. S.; Rong, H. P.; Niu, Z. Q.; Mao, J. J.; Asakura, H.; Tanaka, T.; Dyson, P. J.; Li, J.; Li, Y. D. *Nat. Commun.* **2014**, *5*, 3093.
(65) Huang, X. Q.; Tang, S. H.; Mu, X. L.; Dai, Y.; Chen, G. X.; Zhou, Z. Y.; Ruan, F. X.; Yang, Z. L.; Zheng, N. F. *Nat. Nanotechnol.* **2011**, *6*, 28−32.
(66) Fan, Z. X.; Bosman, M.; Huang, X.; Huang, D.; Yu, Y.; Ong, K. P.; Akimov, Y. A.; Wu, L.; Wu, J.; Liu, Q.; Png, C. E.; Gan, C. L.; Yang, P. D.; Zhang, H. *Nat. Commun.* **2015**, *6*, 7684.
(67) Huang, X.; Li, S. Z.; Huang, Y. Z.; Wu, S. X.; Zhou, X. Z.; Li, S. Z.; Gan, C. L.; Boey, F.; Mirkin, C. A.; Zhang, H. *Nat. Commun.* **2011**, *2*, 292.
(68) Fan, Z. X.; Huang, X.; Han, Y.; Bosman, M.; Wang, Q. X.; Zhu, Y. H.; Liu, Q.; Li, B.; Zeng, Z. Y.; Wu, J.; Shi, W. X.; Li, S. Z.; Gan, C. L.; Zhang, H. *Nat. Commun.* **2015**, *6*, 6571.
(69) Fan, Z. X.; Zhu, Y. H.; Huang, X.; Han, Y.; Wang, Q. X.; Liu, Q.; Gan, C. L.; Zhang, H. *Angew. Chem.* **2015**, *127*, 5764−5768.
(70) Najmaei, S.; Liu, Z.; Zhou, W.; Zou, X. L.; Shi, G.; Lei, S. D.; Yakobson, B. I.; Idrobo, J.-C.; Ajayan, P. M.; Lou, J. *Nat. Mater.* **2013**, *12*, 754−759.
(71) van der Zande, A. M.; Huang, P. Y.; Chenet, D. A.; Berkelbach, T. C.; You, Y. M.; Lee, G.-H.; Heinz, T. F.; Reichman, D. R.; Muller, D. A.; Hone, J. C. *Nat. Mater.* **2013**, *12*, 554−561.
(72) Antolini, E. *Energy Environ. Sci.* **2009**, *2*, 915−931.
(73) Marković, N. M.; Ross, P. N., Jr. *Surf. Sci. Rep.* **2002**, *45*, 117−229.
(74) Li, L. K.; Yu, Y. J.; Ye, G. J.; Ge, Q. Q.; Ou, X. D.; Wu, H.; Feng, D. L.; Chen, X. H.; Zhang, Y. B. *Nat. Nanotechnol.* **2014**, *9*, 372−377.
(75) Rodenas, T.; Luz, I.; Prieto, G.; Seoane, B.; Miro, H.; Corma, A.; Kapteijn, F.; i Xamena, F. X. L.; Gascon, J. *Nat. Mater.* **2015**, *14*, 48−55.


DOI: 10.1021/jacs.5b03590
*J. Am. Chem. Soc.* 2015, 137, 12162−12174

(76) Colson, J. W.; Woll, A. R.; Mukherjee, A.; Levendorf, M. P.; Spitler, E. L.; Shields, V. B.; Spencer, M. G.; Park, J.; Dichtel, W. R. *Science* **2011**, *332*, 228−231.
(77) Tan, C. L.; Qi, X. Y.; Huang, X.; Yang, J.; Zheng, B.; An, Z. F.; Chen, R. F.; Wei, J.; Tang, B. Z.; Huang, W.; Zhang, H. *Adv. Mater.* **2014**, *26*, 1735−1739.
(78) He, D. W.; Zhang, Y. H.; Wu, Q. S.; Xu, R.; Nan, H. Y.; Liu, J. F.; Yao, J. J.; Wang, Z. L.; Yuan, S. J.; Li, Y.; Shi, Y.; Wang, J. L.; Ni, Z. H.; He, L.; Miao, F.; Song, F. Q.; Xu, H. X.; Watanabe, K.; Taniguchi, T.; Xu, J. B.; Wang, X. R. *Nat. Commun.* **2014**, *5*, 5162.
(79) Zhuang, X. D.; Mai, Y. Y.; Wu, D. Q.; Zhang, F.; Feng, X. L. *Adv. Mater.* **2015**, *27*, 403−427.



DOI: 10.1021/jacs.5b03590
*J. Am. Chem. Soc.* 2015, 137, 12162−12174